



Published in final edited form as:

Nano Today. 2014 October ; 9(5): 550–559. doi:10.1016/j.nantod.2014.09.001.

Drug-induced amplification of nanoparticle targeting to tumors

Kevin Y. Lin^a, Ester J. Kwon^b, Justin H. Lo^{c,d}, and Sangeeta N. Bhatia^{b,d,e,f,g,*}

^aDepartment of Chemical Engineering, Massachusetts Institute of Technology, Cambridge, MA 02139

^bHarvard-MIT Division of Health Sciences and Technology, Massachusetts Institute of Technology, Cambridge, MA 02139

^cMedical Scientist Training Program, Harvard Medical School, Boston, MA 02115

^dBroad Institute of Harvard and MIT, Cambridge, MA 02142

^eDepartment of Medicine, Brigham and Women's Hospital, Boston, MA 02115

^fElectrical Engineering and Computer Science, David H. Koch Institute for Integrative Cancer Research, MIT, Cambridge, MA 02139

^gHoward Hughes Medical Institute, Chevy Chase, Maryland 20815, USA

Summary

Nanomedicines have the potential to significantly impact cancer therapy by improving drug efficacy and decreasing off-target effects, yet our ability to efficiently home nanoparticles to disease sites remains limited. One frequently overlooked constraint of current active targeting schemes is the relative dearth of targetable antigens within tumors, which restricts the amount of cargo that can be delivered in a tumor-specific manner. To address this limitation, we exploit tumor-specific responses to drugs to construct a cooperative targeting system where a small molecule therapeutic modulates the disease microenvironment to amplify nanoparticle recruitment *in vivo*. We first administer a vascular disrupting agent, ombrabulin, which selectively affects tumors and leads to locally elevated presentation of the stress-related protein, p32. This increase in p32 levels provides more binding sites for circulating p32-targeted nanoparticles, enhancing their delivery of diagnostic or therapeutic cargos to tumors. We show that this cooperative targeting system recruits over five times higher doses of nanoparticles to tumors and decreases tumor burden when compared with non-cooperative controls. These results suggest that using nanomedicine in conjunction with drugs that enhance the presentation of target antigens in the tumor environment may be an effective strategy for improving the diagnosis and treatment of cancer.

Keywords

Nanomedicine; active targeting; cancer therapy; vascular disrupting agent; liposomes; magnetic nanoworms

*Corresponding author at: Massachusetts Institute of Technology, 77 Massachusetts Avenue, Building 76-453, Cambridge, MA 02139, USA. Tel.: +1 617 324 0610.

1. Introduction

Nanotechnology has enabled numerous novel and improved approaches for cancer diagnosis and therapy. In particular, active targeting of nanoparticles, or the attachment of affinity ligands to the surface of particles to recognize and bind pathological markers, has arisen as an attractive strategy to precisely deliver cargos to disease sites while simultaneously reducing side effects [1]. Efforts to improve the targeting of nanomaterials have largely focused on engineering the properties of individual nanoparticles, including geometry, surface chemistry, ligand type, and ligand density [2–4]. However, one major factor that limits the effectiveness of active targeting is the paucity of targetable antigens available for nanoparticle binding within a tumor [5]. A promising approach for overcoming this limitation is to leverage disease responses to therapy to greatly enhance the number of existing binding sites, or induce the presentation of novel targets. Previously, localized treatments such as radiation [6] and hyperthermia [7, 8] have been used to induce the expression of vascular antigens that serve as binding targets to recruit nanoparticles to tumors. Unfortunately, application of these methods is confined to clinical scenarios where disease sites are known and accessible, and thus preclude the treatment of disseminated disease, which is the primary cause of mortality in cancer [9].

Our strategy is to identify proteins that are selectively induced in the tumor microenvironment following treatment with drugs and leverage them as receptors for targeted nanoparticles. The arsenal of systemic therapies designed to treat metastatic cancer includes traditional cytotoxic drugs [10], molecularly targeted agents [11, 12], immunotherapy [13, 14], and vascular disrupting agents (VDAs) [15, 16], which operate through distinct modes of action. These drugs are attractive inducing agents because many are clinically-approved or in trial stages and are frequently administered in combination with other therapeutics [11, 12, 17]. Drug-induced antigens have been utilized as biomarkers of therapeutic responses or as antibody targets [18–20], but to our knowledge, these changes have never been used to target nanoparticles to tumors. Here, we investigate the ability of systemically administered drugs to increase the prevalence of tumor-specific antigens to amplify nanoparticle targeting to tumors. In this report, we demonstrate that the small molecule VDA, ombrabulin, enhances the presentation of a stress protein called p32 in human tumor xenografts implanted in mice (Figure 1). p32 is specifically expressed in tumors and serves as the target receptor of the cyclic nonapeptide, LyP1, which was discovered through *in vivo* phage display [21, 22]. We then use ombrabulin to induce greater levels of p32 in tumors and deliver two different LyP1-decorated nanoparticles to tumors: a prototypical imaging agent (magnetofluorescent iron oxide nanoworms) and a prototypical therapeutic agent (doxorubicin-loaded liposomes). We show that this cooperative targeting system amplifies the recruitment of targeted nanoparticles to tumors by three- to five-fold over non-cooperative controls, and improves the tumor burden and survival of mice in a preclinical therapeutic study.

2. Results

2.1 Characterization of ombrabulin-induced p32 presentation

Ombrabulin is a microtubule-binding agent that impacts tumor vasculature by effecting a rapid sequence of events shortly after administration, including morphological and functional changes in endothelial cells that increase vascular permeability, and culminate in extensive hemorrhagic necrosis within the tumor [15, 23, 24] (Figure 2A–B). Widespread extravasation of red blood cells into the tumor interstitium was observed within one hour, and central necrosis was evident between six and twenty-four hours following drug administration (Figure 2C). The selective vulnerability of tumor vessels to tubulin-binding compounds has been attributed to their immature development and defective pericyte coverage relative to normal vessels [15, 16]. We hypothesized that the antitumor activity of ombrabulin might increase tumor presentation of p32 [p33/gC1q receptor/hyaluronan binding protein 1 (HABP1)], a mitochondrial protein that is found at elevated levels on the surface of stressed tumor and tumor-associated cells in a wide range of tumor types, particularly in hypoxic or nutrient-deprived regions [22]. To investigate the ability of ombrabulin to increase p32 presentation within tumors, we intravenously injected different doses of the drug (0, 30, 60 mg/kg) into nude mice ($n = 3$ mice per condition) bearing bilateral human MDA-MB-435 tumors. At 4 and 24 hrs, mice were euthanized and p32 presentation was assessed *via* immunofluorescent staining of tumor sections (Figure 2D). We observed that the percentage of p32-positive staining within the tumor trended upward with both time and ombrabulin dose, showing nearly a four-fold increase in p32-positive area at 24 hrs after a 60 mg/kg dose (Figure 2E). To assay for increased p32 presentation at the surface of surviving cancer cells, tumors were dissociated into single cell suspensions for quantification of p32 surface expression by live-cell staining and flow cytometry (Figure S1). Consistent with the trend observed in tumor sections, flow-based examination of the tumor population revealed that the percentage of cancer cells positive for surface p32 increased significantly by up to four-fold at 24 hrs after ombrabulin treatment ($*** P < 0.005$ by one-way ANOVA with Tukey post test; Figure 2F). Together, these data show that exposure to ombrabulin modulates the tumor environment to amplify p32 presentation within the tumor, particularly on the surface of surviving cancer cells.

2.2 Ombrabulin-induced amplification of tumor targeting

We next investigated the ability of magnetofluorescent iron oxide nanoworm (NW) imaging agents, a nanoparticle previously developed by our collaborators [25, 26], to target tumors following ombrabulin treatment (Figure 3A). The NWs were first derivatized with a near-infrared fluorophore (VT750) to enable detection of their distribution by fluorescence imaging. Then, the NWs were further modified by the attachment via PEG of either the cyclic nonapeptide LyP-1 (CGNKRTRGC), which binds p32 and facilitates tissue penetration, or ARAL (ARALPSQRSR), an untargeted peptide that has the same net charge as LyP-1 to control for nonspecific electrostatic interactions of the nanoparticles [7, 22, 27, 28]. The LyP-1 (NW-LyP1) and ARAL (NW-ARAL) conjugated NWs were prepared with similar size distributions and peptide valencies (~40 peptides per NW by absorbance spectroscopy; Figure S2). Additionally, as expected, the NW-LyP1 showed significantly

greater binding to purified recombinant p32 *in vitro* relative to NW-ARAL, which validated the selection of ARAL as a non-targeted control sequence (Figure S3A).

To test for amplification of NW targeting to tumors, different doses of ombrabulin (0, 30, 60 mg/kg) were intravenously injected into mice ($n = 3-4$ mice per condition) bearing bilateral MDA-MB-435 tumors, followed by either NW-LyP1 or NW-ARAL administration after 24 hrs (Figure 3B). At 24 hrs post-NW injection, *ex vivo* fluorescent imaging of tumors revealed a dose-dependent increase in NW-LyP1 accumulation of up to three-fold relative to no drug controls and without altering the organ distribution of the nanoparticles (Figure 3C–D, Figure S4). The non-targeted NW-ARAL also exhibited a marginal dose-dependent increase in accumulation, which is consistent with previous reports demonstrating the enhanced extravasation of macromolecules following vascular disruption by small molecule therapeutics [29]. Notably, the NW-LyP1 exhibited a significantly greater increase in accumulation of $\sim 1.5-2$ fold compared to the NW-ARAL when following ombrabulin treatment ($**P < 0.01$ by Student's *t*-test), which suggested that induction of p32 presentation by ombrabulin leads to amplified targeting of NWs to tumors. Histological examination of tumor sections revealed that the presence of both NW-LyP1 (green) and p32 (red) increased, and localized within ombrabulin-treated tumors (60 mg/kg) versus untreated tumors, while NW-ARAL (green) staining was less intense and did not colocalize with p32 (red) in either scenario (Figure 3E). We also explored an alternative dosing sequence in which ombrabulin and NWs were injected simultaneously and found that co-administration did not lead to a pronounced difference in accumulation between NW-LyP1 and NW-ARAL (Figure S5). This result is consistent with the previous finding that enhancement of p32 presentation takes up to 24 hrs post-ombrabulin treatment, and supports the hypothesis that p32 binding is necessary for the enhanced targeting of NW-LyP1. Collectively, these data show that pre-exposure to ombrabulin mediates the amplification of NW homing to tumors by increasing the amount of the target p32 protein available for binding.

2.3 Ombrabulin-induced amplification of therapeutic delivery

We next constructed model therapeutic nanoparticles, doxorubicin-loaded liposomes (LP), to test for amplified drug delivery to regions of ombrabulin-induced p32 presentation in tumors (Figure 4A). LPs were synthesized with either the targeting peptide LyP1 (LP-LyP1) or the control peptide ARAL (LP-ARAL) on the surface of particles and both populations were confirmed to exhibit similar size distributions (Figure S6) [7]. To test for amplification of LP targeting to tumors, mice ($n = 3$ mice per condition) bearing bilateral MDA-MB-435 tumors were intravenously injected with either saline or ombrabulin (60 mg/kg), followed by LP-LyP1 or LP-ARAL (1 mg/kg by dox) after 24 hrs. At 24 hrs post-LP injection, we found that ombrabulin treatment amplified the delivery of LP-LyP1 and accumulation of doxorubicin in tumors by \sim four-fold versus non-targeted LP-ARAL, ~ 2.5 fold relative to LP-LyP1 alone, and \sim five-fold relative to non-cooperative and non-targeted LP-ARAL ($***P < 0.005$ by Student's *t*-test; Figure 4B). Notably, without ombrabulin, LP-LyP1 also demonstrated higher accumulation of doxorubicin in tumors than LP-ARAL, which was consistent with previous studies using nanoparticles targeted by LyP1 [30–32]. Similar to the NWs, histological examination of tumor sections again showed increased, localized staining of both LP-LyP1 (green) and p32 (red) in ombrabulin-treated tumors versus untreated tumors,

while LP-ARAL (green) staining was sparsely distributed and did not localize to areas with p32 (red) in either scenario (Figure 4C). We also investigated the organ distribution of doxorubicin following cooperative targeting and found that administration of both ombrabulin and LP-LyP1 or LP-ARAL did not change the biodistribution of doxorubicin, with a majority of the drug accumulating in the spleen and liver (Figure 4D). This result indicated that despite being administered systemically, ombrabulin does not lead to the increased accumulation of LPs in off-target sites and that the majority of particles are still cleared by the organs associated with the reticuloendothelial system, which is typical of systemically administered nanomaterials [4]. Altogether, these experiments showed that pre-treatment with ombrabulin amplified the delivery of therapeutic nanoparticles that target the p32 protein.

2.4 Amplified tumor therapy with cooperative therapeutics

Finally, we evaluated the therapeutic efficacy of cooperative targeting in mice ($n = 7$ mice per condition) bearing single MDA-MB-435 human carcinoma tumors. Ombrabulin (60 mg/kg) or saline were injected into mice and 24 hrs later, an intravenous dose of LP-LyP1, LP-ARAL (2 mg/kg by dox), or saline was given. When this treatment regimen was administered every 4–5 days, we found that ombrabulin + LP-LyP1 was significantly more effective at slowing tumor growth ($*P < 0.05$ by two-way ANOVA with Bonferroni post test) than the treatments in isolation (ombrabulin, LP-LyP1, LP-ARAL) and non-cooperative controls (ombrabulin + LP-ARAL; Figure 5A, Figure S7) without any significant changes in animal weight following the last cycle of treatment (Figure 5B). In comparing the long term survival of mice in the various treatment groups, we found that ombrabulin + LP-LyP1 significantly prolonged the survival time of mice relative to all other treatments ($**P < 0.01$ by log rank test, $n = 7$ mice; Figure 5C). Collectively, these therapeutic studies demonstrated that the cooperativity of ombrabulin and targeted LPs led to decreased tumor growth and prolonged survival of mice.

3. Discussion

In this study, we design a cooperative targeting system that harnesses the ombrabulin-induced increase in presentation of p32 to amplify the recruitment of two model nanoparticle systems which are actively targeted to tumors. Using small molecules or proteins to modulate the disease environment is advantageous because they do not face the same extravasation and diffusion barriers as larger vehicles [33], and may therefore effectively prime the tumor microenvironment for subsequent nanoparticle delivery. Numerous related strategies have aimed to enhance nanoparticle accumulation by increasing vascular permeability through the administration of vasoactive agents such as vascular endothelial growth factor, bradykinin, and tumor necrosis factor alpha [34]. However, a general concern with these approaches is that they may affect both healthy and diseased vasculature, thus escalating the risk of off-target effects. In contrast, our method leverages the specificity of ombrabulin for tumor vasculature, which is derived from the increased susceptibility of immature vessels to tubulin-binding agents [15, 16], and the tumor-specific expression of cell-surface p32 to bolster nanoparticle accumulation while simultaneously minimizing off-target delivery [22]. Compared to an earlier study performed by our group using gold

nanorod-mediated hyperthermia, administration of ombrabulin produced a larger increase in the magnitude of tumor p32 expression and a similar fold enhancement in nanoparticle homing to tumors [7]. However, this system offers several advantages over the previously described cooperative system that may impact translation into the clinical setting. First, gold nanorods used in the previous system must overcome significant size-dependent diffusion barriers compared to small molecule VDAs in order to penetrate deep into tumors, actuate the p32 signal throughout the disease site, and facilitate amplified delivery of the second cargo [35]. Additionally, gold nanorod-mediated hyperthermia requires exposing the nanorods to a near-infrared laser, which has a limited penetration depth through tissue (~1 cm), thereby precluding the treatment of tumors located deep within the body [36]. Finally, unlike previous systems that utilize localized and guided treatment modalities such as hyperthermia [7, 8] and radiation therapy [6] to induce the presentation of novel binding sites, our strategy is fully autonomous with the potential to survey the entire body for disseminated disease without any *a priori* knowledge of tumor locations.

Vascular disrupting agents like ombrabulin are attractive inducing agents to use in this cooperative targeting system not only because of their anti-vascular activity against a broad range of tumor types [23, 37], but because preclinical and clinical studies suggest that VDAs have the greatest impact when coupled with other treatments; as single agents, VDAs leave a viable tumor rim that can obtain nutrients and oxygen from neighboring healthy tissues and rapidly re-grow [15, 16, 24]. Here, we demonstrated that pre-treatment of tumors with ombrabulin amplified the delivery of both prototypical diagnostic and therapeutic nanoparticles, highlighting the modularity of this stigmergic targeting approach. This data suggests that this system may be applicable to any number of cargos that are deliverable by nanoparticles, including other chemotherapies, siRNA, or diagnostic markers [1, 2, 38]. Vascular disrupting agents and traditional chemotherapy have previously been coupled together in a single nanoparticle formulation and shown to be therapeutically effective, but these efforts did not incorporate any form of active targeting [39]. Our therapeutic study showed that cooperative targeting was not only more effective than either agent alone, but also was advantageous compared to the combination of ombrabulin and control non-targeted liposomes. These results also suggest that the staggered administration of a cooperative combination of drug and targeted nanoparticle may generate positive therapeutic indices by enhancing the delivery of cargos. Furthermore, recent studies have highlighted the importance of optimizing the dosing schedule for combination therapies involving VDAs given their range of temporal effects, with most recent results supporting the pretreatment of tumors with VDA prior to chemotherapy [40, 41]. The protocol and results of our cooperative strategy were consistent with these findings, showing a greater enhancement in nanoparticle accumulation when they were administered 24 hrs after ombrabulin versus when they were co-administered.

Looking forward, several experimental avenues warrant further investigation in order to expand the applicability of cooperative nanoparticle targeting. In this study, we used a VDA to increase the number of nanoparticle binding sites within tumors, however the current arsenal of cancer treatments includes many other candidates with the potential to serve as inducing agents for cooperative targeting approaches. In addition to the aforementioned treatment modalities, traditional chemotherapies and next-generation targeted therapies have

also been used to induce tumor antigens, which were identified by either gene expression profiling [20, 42] or *in vivo* phage display [18, 19]. Future studies may focus on developing systematic screening approaches to identify novel induced antigens in response to panels of drugs spanning multiple classes. These antigens could then be cross-referenced to known libraries of targeting ligands from the literature or used to develop new ligands in order to create more potential pairings of cooperative drugs and ligand-decorated nanoparticles. In summary, this work introduces a new approach for designing nanoparticle targeting systems that leverages drug-induced modulation of the disease environment to improve the detection and treatment of cancer.

4. Materials & Methods

Generation of MDA-MB-435 xenografts

MDA-MB-435 cancer cell lines (American Type Culture Collection) were cultured in Dulbecco's Modified Eagle Medium (DMEM) with 10% fetal bovine serum, penicillin, and streptomycin. To generate subcutaneous xenograft models, 4–6 week old female NCr nude mice (Taconic) were injected either laterally or bilaterally in the hind flanks, according to the experimental design, with $\sim 2 \times 10^6$ MDA-MB-435 cells suspended in 200 μ L DMEM.

Histological analysis

Omrabulin was kindly provided by Sanofi Aventis. Mice bearing bilateral flank MDA-MB-435 xenografts (n = 3 mice) were intravenously administered different dosages of omrabulin (0, 30, 60 mg/kg) in 0.9% NaCl without anesthesia. At different time points (4, 24 hrs p.i.) the mice were euthanized and their tumors were excised. For hematoxylin and eosin staining, tumors were fixed in 4% paraformaldehyde for 1–2 hours at RT and stored in 70% ethanol until paraffin-embedding, sectioning, and staining (Koch Institute Histology Core). For immunofluorescent staining, representative frozen tumor sections were stained for p32 (Millipore) and Hoechst (Invitrogen) before analysis by fluorescence microscopy (Nikon Eclipse Ti). The percentage of p32 positive staining in the tumor was quantified using MATLAB (MathWorks).

Flow cytometry

Omrabulin (0, 30, or 60 mg/kg) was administered intravenously to mice bearing bilateral flank MDA-MB-435 xenografts. At different time points (4 or 24 hrs post-injection), the mice were euthanized and their tumors were excised in their entirety. The tumors were gently dissociated into single cell suspensions using a MACS human Tumor Dissociation Kit (Miltenyi Biotec) according to manufacturer instructions. 2.5×10^6 cells per condition were incubated for 1 hr on ice with both Alexa Fluor-488-conjugated mouse anti-human HLA-AB (BD Pharmingen) and either rabbit polyclonal anti-p32 (Millipore) or rabbit IgG isotype control (R&D Systems). Cells were then washed twice with cold PBS supplemented with 2% fetal bovine serum (FBS), followed by incubation for 1 hr on ice with Alexa Fluor-594 goat anti-rabbit secondary antibody (Invitrogen). Cells were washed and then resuspended in PBS plus 2% FBS for analysis. For quantification of surface p32 levels, human tumor cells were isolated by gating out all HLA-ABC-negative cells.

Peptide nanoworm synthesis

Aminated iron oxide NWs were synthesized according to previously published protocols [26]. Peptides (LyP1 = C-(K-Flsc)-C6-CGNKRTRGC, Cys2 & Cys3 bridge; ARAL = C-(K-Flsc)-C6-ARALPSQRSR; Flsc = fluorescein, C6 = 6-aminohexanoic acid linker) were synthesized by CPC Scientific and the Tufts University Core Facility peptide synthesis service. To conjugate peptides to NWs, NWs were first reacted with NHS-VivoTag 750 (VT750, PerkinElmer) and MAL-PEG(5k)-SVA (Laysan Bio.) to introduce sulfhydryl-reactive handles. Cysteine terminated peptides were then mixed with NWs (95:1 molar ratio) for one hour at room temperature (RT) and purified using a Sephadex G-25 gel filtration column (GE Healthcare). Stock solutions were stored in PBS at 4°C. The number of fluorescein-labeled peptides per NWs was determined by absorbance spectroscopy using the absorbance of fluorescein (490 nm) and its extinction coefficient ($78,000 \text{ cm}^{-1}\text{M}^{-1}$). The particle size was measured by dynamic light scattering (Malverin Zetasizer Nano Series).

Doxorubicin-loaded liposome synthesis

Hydrogenated soy sn-glycero-3-phosphocholine (HSPC), cholesterol, and 1,2-distearoyl-sn-glycero-3-phosphoethanolamine-N-polyethylene glycol 2000 [DSPE-PEG(2k)] were purchased from Avanti Polar Lipids. DSPE-[Maleimide(Polyethylene Glycol 5000)] [DSPE-PEG(5K)-MAL] was purchased from Nanocs, Inc. Doxorubicin was purchased from Sigma Chemical Co. For peptide conjugation, DSPE-PEG(5K)-MAL was reacted with Cysteine-terminated peptides (LyP1 or ARAL) in 50 mM triethylamine, DMF for 24 hours and exchanged into water using gel filtration. Liposomes were prepared from HSPC, cholesterol, and either DSPE-PEG(5K)-LyP1 or DSPE-PEG(5K)-ARAL in the molar ratio of 75:50:3 by lipid film hydration and membrane (100 nm) extrusion method [43]. Encapsulation of doxorubicin (dox) into the liposomes was then carried out using the pH gradient-driven loading protocol [44]. Free doxorubicin was removed by gel filtration on Sephadex G-25. The peptide-conjugated doxorubicin liposomes were stored in PBS at 4 °C before use. The particle size was measured by dynamic light scattering (Malverin Zetasizer Nano Series) and the fluorescence intensity was measured by microplate reader (SpectroMax Gemini EM, Molecular Devices).

In vitro binding assay

The *in vitro* binding of nanoparticles to p32 was assessed using a magnetic bead assay. Briefly, NWs (40 pmol by Flsc) or LPs (1.5 pmol by Flsc) were incubated with Ni-NTA magnetic agarose beads (Qiagen) coated with His-tagged recombinant p32 protein (kindly provided by Dr. T. Teesalu) in binding and washing buffer (BWB; PBS with 300 mM NaCl, 5 mM imidazole, 0.05% NP-40, 0.1% bovine serum albumin) for 1 hr at room temperature, washed four times with BWB, and eluted with 400 mM imidazole in BWB. Samples were quantified by fluorescence microplate reader (SpectroMax Gemini EM, Molecular Devices) at excitation/emission wavelengths of 485/538 nm and compared to standard curves.

Nanoworm homing to tumors

Mice bearing bilateral flank MDA-MB-435 xenografts (n = 3–4 mice) were intravenously administered different dosages of ombrabulin (0, 30, 60 mg/kg). NW-LyP1 or NW-ARAL (1

nmol by VT750) were either co-administered or injected 24 hrs following ombrabulin administration. At 24 hrs post-NW administration, organs were removed and scanned on the LI-COR Odyssey Infrared Imaging System. Fluorescence in each organ was quantified using ImageJ software (NIH). To analyze tumors by immunostaining, representative sections were stained for NWs (anti-Flsc primary, GeneTex), either p32 (Millipore) or CD31 (BD Pharmingen), and Hoechst (Invitrogen) before analysis by fluorescence microscopy (Nikon Eclipse Ti).

Quantification of doxorubicin in tissues

Mice bearing bilateral flank MDA-MB-435 xenografts (n = 3 mice) were intravenously administered different dosages of ombrabulin (0, 60 mg/kg), followed by either LP-LyP1 or LP-ARAL (1 mg/kg by dox) 24 hours later. At 24 hrs post-LP administration, organs were removed, weighed, incubated with 500 μ l of 70% EtOH, 0.3 N HCl, and homogenized (Tissue Tearor, Biospec Products) to release doxorubicin from tissues. Following homogenization, another 1 ml of 70% EtOH, 0.3 N HCl, was added to samples and they were centrifuged. Supernatants of samples were analyzed for doxorubicin fluorescence using a fluorescence microplate reader (SpectroMax Gemini EM, Molecular Devices) at excitation/emission wavelengths of 470/590 nm and compared to standard curves. To analyze tumors by immunostaining, representative sections were stained for LPs (anti-Flsc primary, GeneTex), p32 (Millipore), and Hoechst (Invitrogen) before analysis by fluorescence microscopy (Nikon Eclipse Ti).

Therapeutic assessment of cooperative targeting systems

Treatment of mice commenced fourteen days after subcutaneous injection of MDA-MB-435 cancer cells. Tumor dimensions were measured with calipers and the volume was calculated using the modified ellipsoid formula ($\text{volume} = 1/2 \times \text{length} \times \text{width}^2$), where L and W refer to the larger and smaller perpendicular dimensions collected at each measurement [45]. Mice bearing single lateral xenografts were randomized into groups of seven mice such that the mean tumor volumes were similar between groups. Mice were first administered different dosages of ombrabulin (0, 60 mg/kg). At 24 hrs post-injection, mice were administered LP-LyP1 (2 mg/kg), LP-ARAL (2 mg/kg), or saline. This treatment regimen was repeated every 4–5 days. At regular intervals after treatment, tumors were measured and mice were weighed. For the survival curve study, mice were sacrificed when tumors exceeded the humane endpoint set at 500 mm³. To compute the volumetric doubling time of tumors, each tumor volume trace was fit to an exponential growth curve in Excel (Microsoft) and the doubling time was calculated from the growth constant [46].

Statistical analyses

Student's *t*-test, one- and two-way ANOVA, and survival curve analyses were calculated with GraphPad 5.0 (Prism).

All experimental protocols involving animals were approved by the MIT Committee on Animal Care (protocol #0411-036-14).

Supplementary Material

Refer to Web version on PubMed Central for supplementary material.

Acknowledgments

We thank Joerg Adamczewski, Hichem Chakroun, Patricia Vrignaud, and Chantal Carrez from Sanofi-Aventis for generously providing us with ombrabulin and experimental guidance. We thank Dr. Tabet Teesalu for providing us with recombinant p32. We thank the Koch Institute Swanson Biotechnology Center (MIT) for assistance with tissue sectioning, specifically Michael Brown and Kathleen Cormier from the Histology core. We thank Dr. Heather Fleming (MIT) for critical readings of the manuscript. This work was supported by the NIH (BRP: R01CA124427-01), NIH/NCI (U54CA119349, U54CA119335, and the Alliance Challenge Project/MIT-Harvard Center of Cancer Nanotechnology Excellence: U54CA151884), Packard Fellowship (1999-1453), and Marie-D. & Pierre Casimir-Lambert Fund. This work was supported in part by the Koch Institute Support (core) Grant P30-CA14051 from the National Cancer Institute. K.Y.L. acknowledges support from CCNE (5 U54 CA151884-03). J.H.L. acknowledges support from NIH MSTP program (T32GM007753). Dr. E.J.K. acknowledges support from the Ruth L. Kirschstein National Research Service Award (1F32CA177094-01). Dr. S.N.B. is an HHMI Investigator.

References

1. Ferrari M. *Nat. Rev. Cancer.* 2005; 5:161–171. [PubMed: 15738981]
2. Petros RA, DeSimone JM. *Nat. Rev. Drug Discov.* 2010; 9:615–627. [PubMed: 20616808]
3. Byrne JD, Betancourt T, Brannon-Peppas L. *Adv. Drug. Deliv. Rev.* 2008; 60:1615–1626. [PubMed: 18840489]
4. Li S-D, Huang L. *Mol. Pharm.* 2008; 5:496–504. [PubMed: 18611037]
5. Ruoslahti E, Bhatia SN, Sailor MJ. *J. Cell Biol.* 2010; 188:759–768. [PubMed: 20231381]
6. Hallahan D, Geng L, Qu S, Scarfone C, Giorgio T, Donnelly E, Gao X, Clanton J. *Cancer Cell.* 2003; 3:63–74. [PubMed: 12559176]
7. Park J-H, von Maltzahn G, Xu MJ, Fogal V, Kotamraju VR, Ruoslahti E, Bhatia SN, Sailor MJ. *Proc. Natl. Acad. Sci. U. S. A.* 2010; 107:981–986. [PubMed: 20080556]
8. von Maltzahn G, Park J-H, Lin KY, Singh N, Schwöppe C, Mesters R, Berdel WE, Ruoslahti E, Sailor MJ, Bhatia SN. *Nat. Mater.* 2011; 10:545–552. [PubMed: 21685903]
9. Chambers AF, Groom AC, MacDonald IC. *Nat. Rev. Cancer.* 2002; 2:563–572. [PubMed: 12154349]
10. Chabner BA, Roberts TG Jr. *Nat. Rev. Cancer.* 2005; 5:65–72. [PubMed: 15630416]
11. Kummar S, Chen HX, Wright J, Holbeck S, Millin MD, Tomaszewski J, Zweibel J, Collins J, Doroshow JH. *Nat. Rev. Drug Discov.* 2010; 9:843–856. [PubMed: 21031001]
12. Al-Lazikani B, Banerji U, Workman P. *Nat. Biotechnol.* 2012; 30:679–692. [PubMed: 22781697]
13. Weiner LM, Surana R, Wang S. *Nat. Rev. Immunol.* 2010; 10:317–327. [PubMed: 20414205]
14. Mellman I, Coukos G, Dranoff G. *Nature.* 2011; 480:480–489. [PubMed: 22193102]
15. Tozer GM, Kanthou C, Baguley BC. *Nat. Rev. Cancer.* 2005; 5:423–435. [PubMed: 15928673]
16. Heath VL, Bicknell R. *Nat. Rev. Clin. Oncol.* 2009; 6:395–404. [PubMed: 19424102]
17. DeVita VT Jr, Young RC, Canellos GP. *Cancer.* 1975; 35:98–110. [PubMed: 162854]
18. Han Z, Fu A, Wang H, Diaz R, Geng L, Onishko H, Hallahan DE. *Nat. Med.* 2008; 14:343–349. [PubMed: 18297085]
19. Passarella RJ, Zhou L, Phillips JG, Wu H, Hallahan DE, Diaz R. *Clin. Cancer Res.* 2009; 15:6421–6429. [PubMed: 19825959]
20. Rubinfeld B, Upadhyay A, Clark SL, Fong SE, Smith V, Koeppen H, Ross S, Polakis P. *Nat. Biotechnol.* 2006; 24:205–209. [PubMed: 16444269]
21. Laakkonen P, Porkka K, Hoffman JA, Ruoslahti E. *Nat. Med.* 2002; 8:751–755. [PubMed: 12053175]
22. Fogal V, Zhang L, Krajewski S, Ruoslahti E. *Cancer Res.* 2008; 68:7210–7218. [PubMed: 18757437]

23. Morinaga Y, Suga Y, Ehara S, Harada K, Nihei Y, Suzuki M. *Cancer Sci.* 2003; 94:200–204. [PubMed: 12708497]
24. Dumontet C, Jordan MA. *Nat. Rev. Drug Discov.* 2010; 9:790–803. [PubMed: 20885410]
25. Park J-H, Maltzahn Gv, Zhang L, Schwartz MP, Ruoslahti E, Bhatia SN, Sailor MJ. *Adv. Mater.* 2008; 20:1630–1635. [PubMed: 21687830]
26. Park J-H, von Maltzahn G, Zhang L, Derfus AM, Simberg D, Harris TJ, Ruoslahti E, Bhatia SN, Sailor MJ. *Small.* 2009; 5:694–700. [PubMed: 19263431]
27. Ren Y, Cheung HW, von Maltzahn G, Agrawal A, Cowley GS, Weir BA, Boehm JS, Tamayo P, Karst AM, Liu JF, Hirsch MS, Mesirov JP, Drapkin R, Root DE, Lo J, Fogal V, Ruoslahti E, Hahn WC, Bhatia SN. *Sci. Transl. Med.* 2012; 4:147ra112.
28. Roth L, Agemy L, Kotamraju VR, Braun G, Teesalu T, Sugahara KN, Hamzah J, Ruoslahti E. *Oncogene.* 2012; 31:3754–3763. [PubMed: 22179825]
29. Tozer GM, Prise VE, Wilson J, Cemazar M, Shan S, Dewhurst MW, Barber PR, Vojnovic B, Chaplin DJ. *Cancer Res.* 2001; 61:6413–6422. [PubMed: 11522635]
30. Åkerman ME, Chan WCW, Laakkonen P, Bhatia SN, Ruoslahti E. *Proc. Natl. Acad. Sci. U. S. A.* 2002; 99:12617–12621. [PubMed: 12235356]
31. Karmali PP, Kotamraju VR, Kastantin M, Black M, Missirlis D, Tirrell M, Ruoslahti E. *Nanomed: Nanotechnol. Biol. Med.* 2009; 5:73–82.
32. von Maltzahn G, Ren Y, Park J-H, Min D-H, Kotamraju VR, Jayakumar J, Fogal V, Sailor MJ, Ruoslahti E, Bhatia SN. *Bioconjug. Chem.* 2008; 19:1570–1578. [PubMed: 18611045]
33. Yuan F, Dellian M, Fukumura D, Leunig M, Berk DA, Torchilin VP, Jain RK. *Cancer Res.* 1995; 55:3752–3756. [PubMed: 7641188]
34. Cheng Z, Al Zaki A, Hui JZ, Muzykantov VR, Tsourkas A. *Science.* 2012; 338:903–910. [PubMed: 23161990]
35. Jain RK, Stylianopoulos T. *Nature reviews. Clinical oncology.* 2010; 7:653–664.
36. Wilson BC, Jacques SL. *Ieee J Quantum Elect.* 1990; 26:2186–2199.
37. Nihei Y, Suga Y, Morinaga Y, Ohishi K, Okano A, Ohsumi K, Hatanaka T, Nakagawa R, Tsuji T, Akiyama Y, Saito S, Hori K, Sato Y, Tsuruo T. *Cancer Sci.* 1999; 90:1016–1025.
38. Davis ME, Zuckerman JE, Choi CH, Seligson D, Tolcher A, Alabi CA, Yen Y, Heidel JD, Ribas A. *Nature.* 2010; 464:1067–1070. [PubMed: 20305636]
39. Sengupta S, Eavarone D, Capila I, Zhao G, Watson N, Kiziltepe T, Sasisekharan R. *Nature.* 2005; 436:568–572. [PubMed: 16049491]
40. Martinelli M, Bonezzi K, Riccardi E, Kuhn E, Frapolli R, Zucchetti M, Ryan AJ, Taraboletti G, Giavazzi R. *Br. J. Cancer.* 2007; 97:888–894. [PubMed: 17848949]
41. Wang ES, Pili R, Seshadri M. *J. Clin. Oncol.* 2012; 30:760–761. [PubMed: 22291088]
42. Tice DA, Szeto W, Soloviev I, Rubinfeld B, Fong SE, Dugger DL, Winer J, Williams PM, Wieand D, Smith V, Schwall RH, Pennica D, Polakis P. *J. Biol. Chem.* 2002; 277:14329–14335. [PubMed: 11832495]
43. Hope MJ, Bally MB, Webb G, Cullis PR. *Biochim. Biophys. Acta.* 1985; 812:55–65. [PubMed: 23008845]
44. Mayer LD, Bally MB, Hope MJ, Cullis PR. *Biochim. Biophys. Acta.* 1985; 816:294–302. [PubMed: 3839135]
45. Euhus DM, Hudd C, Laregina MC, Johnson FE. *J. Surg. Oncol.* 1986; 31:229–234. [PubMed: 3724177]
46. Schwartz M. *Cancer.* 1961; 14:1272–1294. [PubMed: 13909709]

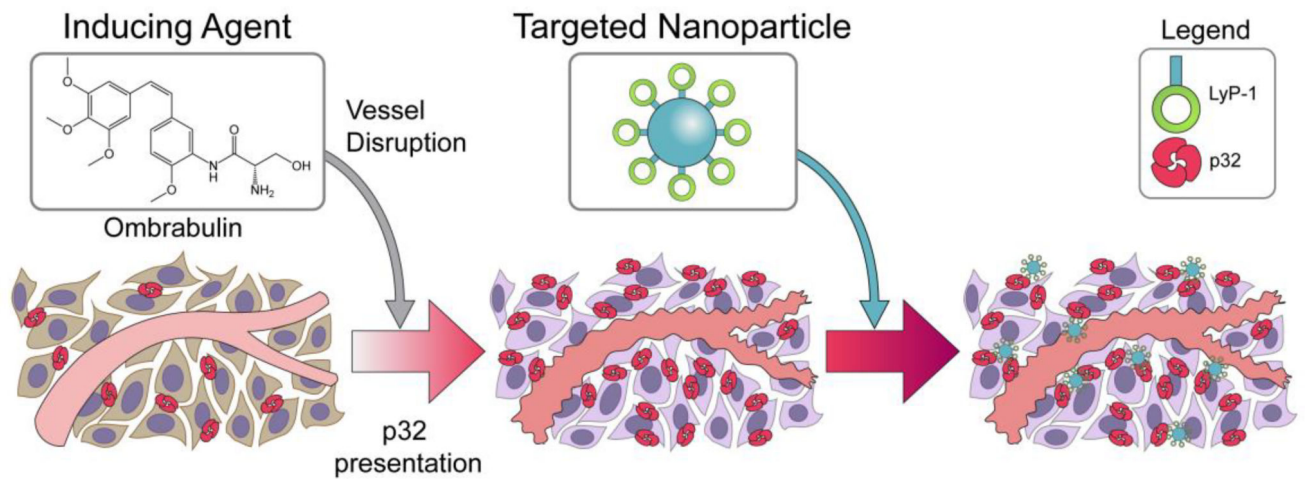
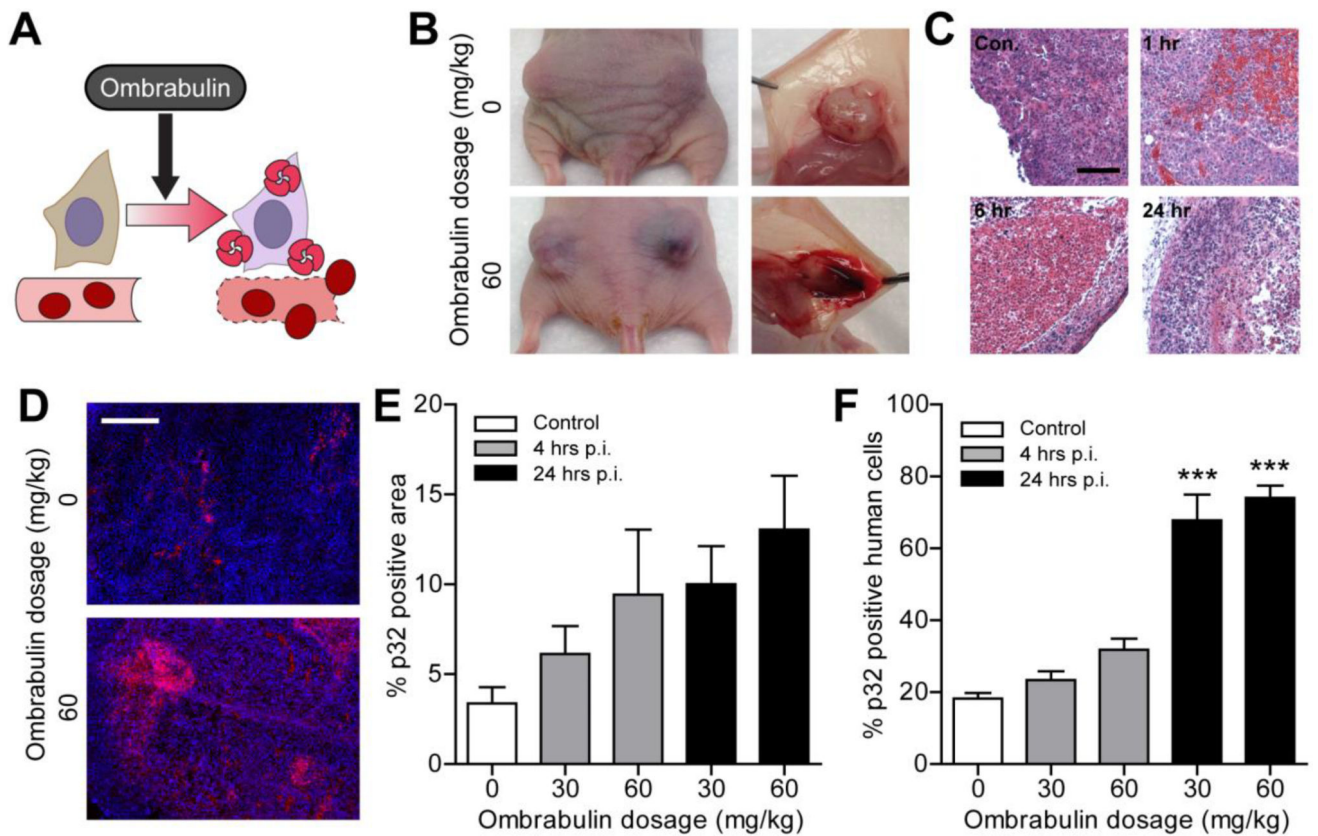


Figure 1. Schematic of cooperative targeting approach

Inducing agent, ombrabulin, disrupts the tumor vasculature, which initiates a cascade of intratumoral effects that lead to upregulated presentation of the p32 protein. LyP-1 coated nanoparticles, which target the p32 protein, are then able to home to the tumor.



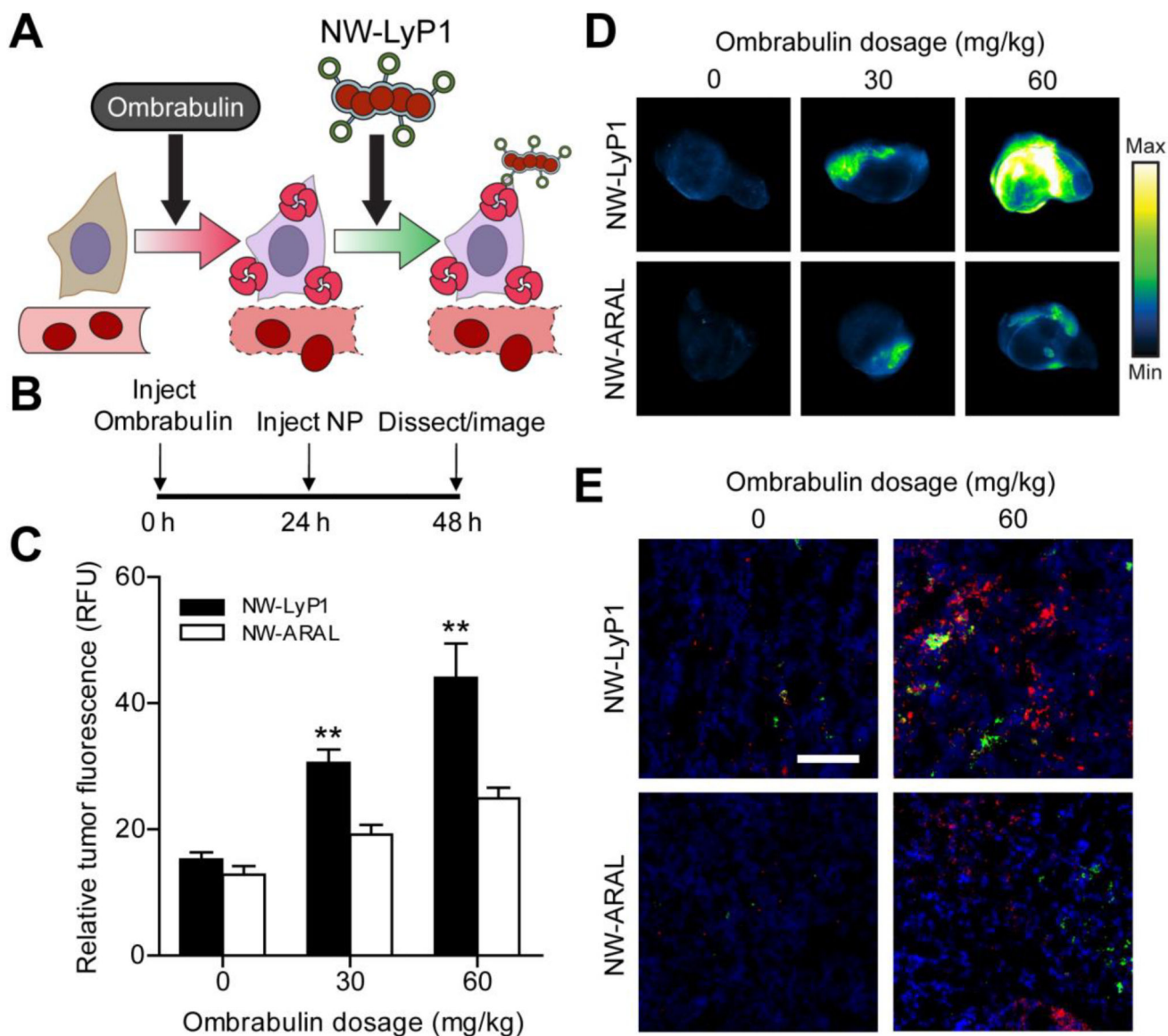


Figure 3. Ombrabulin mediated amplification of NW delivery

(A) Schematic of ombrabulin signaling to NWs. Ombrabulin upregulates the presentation of p32 in tumors, which is then targeted by NW-LyP1. (B) Experimental timeline for testing the signaling system. (C) Quantification of NW homing to tumors as a function of ombrabulin dosage (** $P < 0.01$, Student's *t*-test; $n = 3-4$ mice, s.e.). (D) Representative near-infrared fluorescent scans of NW homing to tumors in response to increasing doses of ombrabulin. Tumors were excised and imaged at 24 hrs post-NW injection. (E) Immunofluorescent staining of NWs in tumors without (0 mg/kg) and with (60 mg/kg) ombrabulin (green = NW, red = p32 staining, blue = nuclear stain; scale bar = 100 μm).

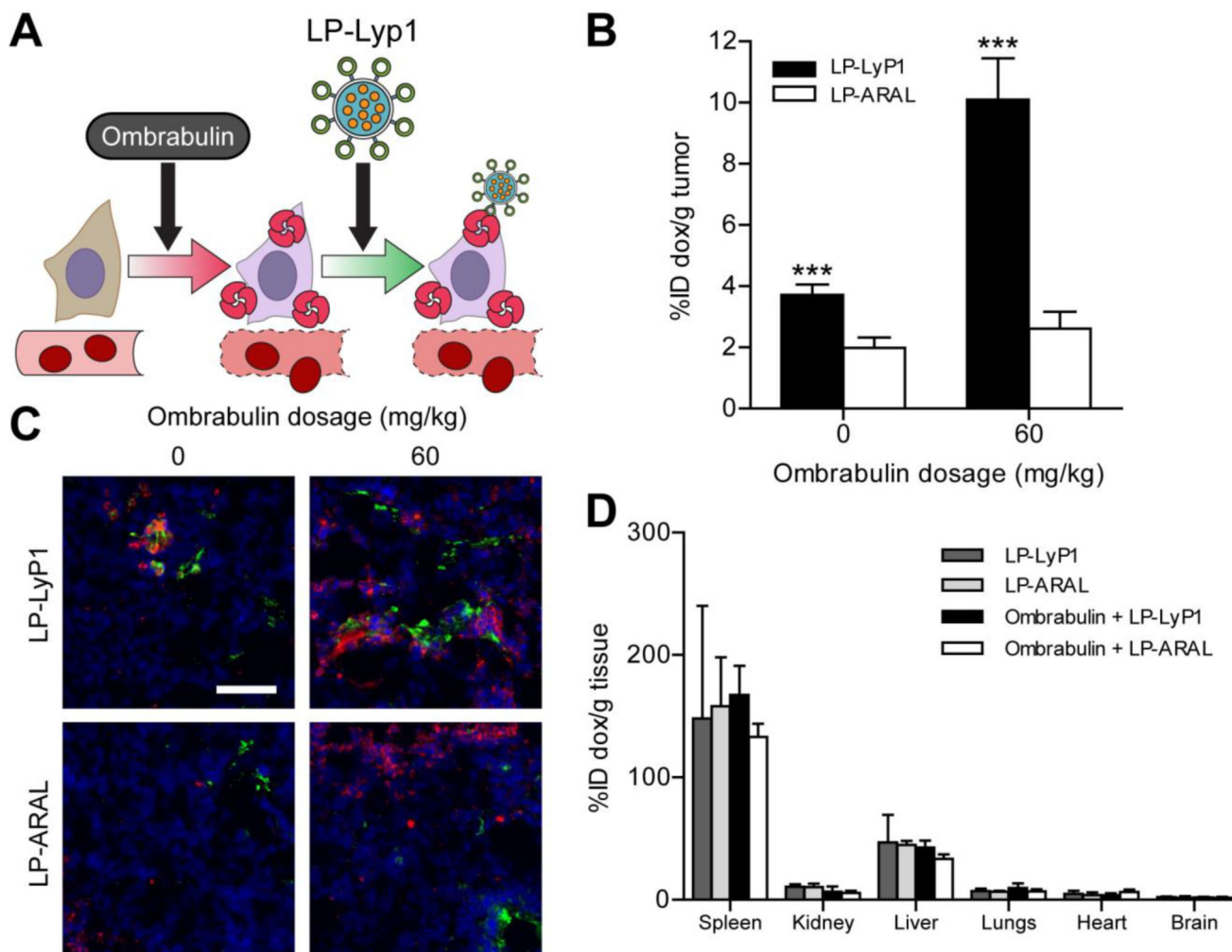


Figure 4. Ombrabulin mediated amplification of LP delivery

(A) Schematic of ombrabulin signaling to LPs. Ombrabulin upregulates the presentation of p32 in tumors, which is then targeted by LP-LyP1. (B) Quantification of doxorubicin-loaded LP homing to tumors as a function of ombrabulin dosage (*** $P < 0.005$, Student's t -test; $n = 3$ mice, s.e.). (C) Immunofluorescent staining of LPs in tumors without (0 mg/kg) and with (60 mg/kg) ombrabulin (green = LP, red = p32 staining, blue = nuclear stain; scale bar = 100 μm). (D) Quantification of doxorubicin-loaded LP biodistribution in organs without (0 mg/kg) and with (60 mg/kg) ombrabulin (No significance, one-way ANOVA with Tukey post test; $n = 3-6$ mice, s.d.).

